

EXAFS studies of the local environment of lead and selenium atoms in $\text{PbTe}_{1-x}\text{Se}_x$ solid solution

A. I. Lebedev, I. A. Sluchinskaya, and V. N. Demin
M. V. Lomonosov Moscow State University, 119899 Moscow, Russia

I. Munro
Daresbury Laboratory, Warrington WA4 4AD, UK

EXAFS spectroscopy is used to study the local environment of lead and selenium atoms in $\text{PbTe}_{1-x}\text{Se}_x$ solid solution. In addition to a bimodal distribution of bond lengths in the first shell, unusually large Debye–Waller factors for the Pb–Pb interatomic distances in the second shell and a substantial deviation of these distances from Vegard’s law are observed. Valence force field (VFF) calculations show that these observations are due to the complex structure of the distribution function for Pb–Pb distances. It is found that the number of Se–Se pairs in the second shell surpasses the statistical value, which indicates that chemical factors play an important role in the structure of the solid solution. The contribution of these chemical factors to the enthalpy of mixing of the solid is estimated to be approximately 0.5 kcal/mole, which is comparable to the strain contribution.

Published in *Physics of the Solid State* **41**, 1275 (1999).

1. INTRODUCTION

Knowledge of the true structure of solid solutions, i.e., the local displacements of atoms from their ideal positions in a lattice and the deviations of atomic distribution from the statistical one is needed to understand the physical properties of these crystals. EXAFS spectroscopy is now widely used for studying the structure of solid solutions.

EXAFS (extended x-ray-absorption fine-structure) studies of solid solutions of III–V and II–VI semiconductors with a zinc blende structure [1–6] have revealed a bimodal distribution of bond lengths in the first shell. This suggests that the fixed chemical bond length approximation proposed by Bragg and Pauling is more suitable for describing the local structure of solid solutions rather than the virtual crystal approximation. Up to now, solid solutions of IV–VI semiconductors with the rocksalt NaCl structure have been studied by EXAFS only to examine the locations of off-center impurities [7–10], no systematic investigations of the local structure have been made for these solid solutions that contain no off-center impurities.

In this work, the results of an EXAFS study of the local structure of the $\text{PbTe}_{1-x}\text{Se}_x$ solid solution are presented. This solid solution is of particular interest due to its use in creating IR optoelectronic devices, specifically as a material for lattice-matched heterojunctions. The binary compounds PbTe and PbSe form a continuous series of solid solutions across the entire composition range, with lattice parameters of 6.460 and 6.126 Å at 300 K, respectively. Their solid solution is characterized by a relatively large difference in the bond lengths (approximately 5%). Additionally, this solid solution is of interest due to the fact that at $x \approx 0.25$ its lattice exhibits a maximum “softening” in respect to the onset of

the ferroelectricity when doped with Sn atoms [11].

2. EXPERIMENTAL DETAILS

Samples of $\text{PbTe}_{1-x}\text{Se}_x$ solid solution with $x = 0.1, 0.25, 0.5,$ and 0.75 were prepared by alloying stoichiometric PbTe and PbSe binary compounds in evacuated silica ampoules with subsequent homogenizing annealing at 720°C for 170 h. X-ray analysis found all the samples to be single-phase. Just before the EXAFS measurements, the samples were ground, the obtained powders were sifted through a mesh and deposited on a scotch tape. An optimum thickness of the absorbing layer for taking spectra was obtained by multiple folding the tape (usually 8 layers).

The EXAFS measurements were carried out on the station 7.1 of the Daresbury synchrotron radiation source (Great Britain) with an electron beam energy of 2 GeV and a maximum stored current of 230 mA. Data were collected at the K absorption edge of Se (12658 eV) and the L_{III} absorption edge of Pb (13055 eV) at 80 K in the transmission mode. The synchrotron radiation was monochromatized by a double-crystal Si(111) monochromator. The intensities of the incident radiation (I_0) and the radiation transmitted through the sample (I_t) were measured by ionization chambers filled with He+Ar mixtures, which absorb 20 and 80% of the x-ray radiation, respectively. Contamination of the incident radiation by higher harmonics can be neglected in the energy range used in the experiments.

The obtained transmission spectra $\mu x(E) = \ln(I_0/I_t)$ (where E is the photon energy) were analyzed in the usual way [12]. After subtracting the pre-edge background, splines were used to extract a smooth atomic part of absorption $\mu x_0(E)$, and then the EXAFS function, $\chi = (\mu x - \mu x_0)/\mu x_0$, was calculated as a function of

the photoelectron wave vector $k = [2m(E - E_0)/\hbar^2]^{1/2}$. The energy origin, E_0 , was determined by the position of the inflection point on the absorption edge. The edge steps ranged from 0.08 to 1.4. At least two independent measurements were taken for each sample.

When multiple scattering effects are neglected, information on the local environment of the central atom, i.e., the distances R_j , coordination numbers N_j , and Debye–Waller factors σ_j^2 for each j th shell enters the EXAFS function as follows [12]:

$$\chi(k) = \frac{1}{k} \sum_j \frac{N_j S_0^2}{R_j^2} f(k) \exp\left(-\frac{2R_j}{\lambda(k)} - 2k^2 \sigma_j^2\right) \times \sin[2kR_j + \psi(k)]. \quad (1)$$

In addition to the structural parameters characterizing the local environment, this equation also includes the amplitude $f(k)$, the sum of the backscattering and central atoms' phase shifts $\psi(k)$, the photoelectron mean free path $\lambda(k)$, and the amplitude reduction factor S_0^2 , which accounts for many-electron and inelastic effects in the central and scattering atoms. The functions $f(k)$, $\psi(k)$, and $\lambda(k)$ were calculated using the FEFF5 program [13].

The information about two the nearest shells from the experimental $\chi(k)$ curves was isolated using forward and inverse Fourier transforms with Hamming windows. The structural parameters R_j , N_j , and σ_j^2 for the two shells as well as the energy origin correction dE_0 were determined by minimizing the root-mean-square deviation between the experimental and calculated $k\chi(k)$ curves using a modified Levenberg–Marquardt algorithm. The number of fitting parameters (8–9) was approximately half the number of independent data points ($2\Delta k \Delta R/\pi = 12\text{--}20$, where Δk and ΔR are the range widths used for Fourier filtration in k and R spaces [12]). The accuracy of the fitting parameters was estimated from the covariance matrix, and the reported errors correspond to the standard deviation. To improve accuracy, it was assumed that the dE_0 correction energy is the same for all shells and that the coordination numbers correspond to the known coordination numbers in a fcc lattice.

3. EXPERIMENTAL RESULTS

Fig. 1 displays typical $k\chi(k)$ curves obtained at the Se K absorption edge for $\text{PbTe}_{1-x}\text{Se}_x$ and PbSe . The maximum wave number for these data is limited by $k \approx 9.7 \text{ \AA}^{-1}$ due to the proximity of the L_{III} absorption edge of Pb. Fig. 2 shows typical $k\chi(k)$ curves obtained at the Pb L_{III} absorption edge for $\text{PbTe}_{1-x}\text{Se}_x$, PbTe , and PbSe . Sharp jumps on the curves marked by arrows at $k \approx 8.7 \text{ \AA}^{-1}$ in Fig. 1 and $k \approx 6.2$ and 12.7 \AA^{-1} on Fig. 2, the so-called glitches, are artifacts arising from the monochromator and do not reflect the properties of

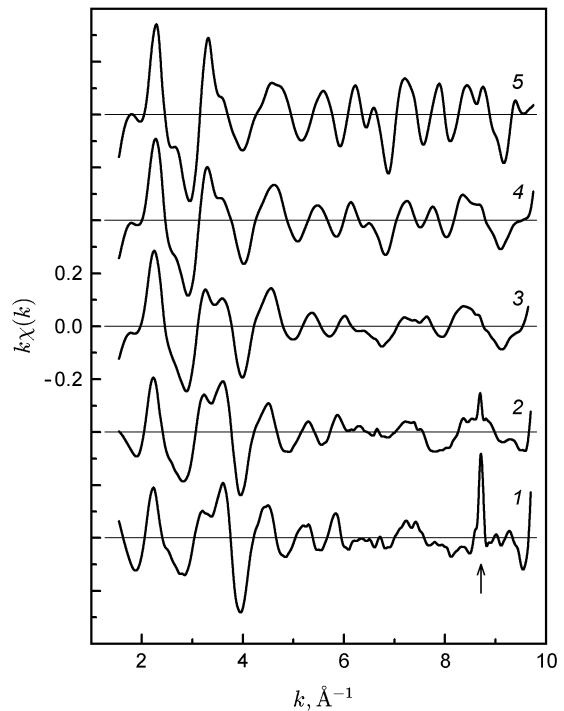


FIG. 1. EXAFS $k\chi(k)$ spectra obtained at the K absorption edge of Se for $\text{PbTe}_{1-x}\text{Se}_x$ samples. x : 1 — 0.1, 2 — 0.25, 3 — 0.5, 4 — 0.75, 5 — 1. The arrow denotes the location of a glitch.

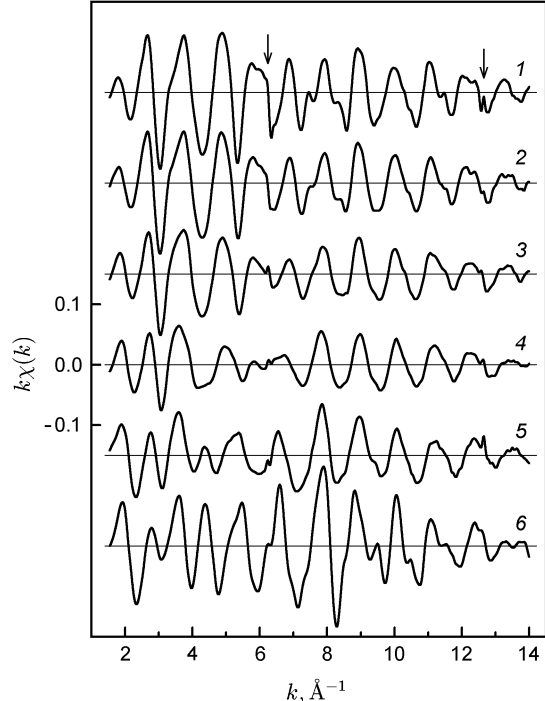


FIG. 2. EXAFS $k\chi(k)$ spectra obtained at the L_{III} absorption edge of Pb for $\text{PbTe}_{1-x}\text{Se}_x$ samples. x : 1 — 0, 2 — 0.1, 3 — 0.25, 4 — 0.5, 5 — 0.75, 6 — 1. The arrows indicate the locations of glitches.

TABLE I. Local concentration of Se–Se pairs in the $\text{PbTe}_{1-x}\text{Se}_x$ solid solution.

x	0.1	0.25	0.5	0.75	1.0
$N_{\text{Se-Se}}/12$	0.34 ± 0.04	0.45 ± 0.03	0.60 ± 0.02	0.78 ± 0.01	0.96 ± 0.02

the sample. After deglitching, the data were processed as described in the previous section.

In analyzing data, we have limited ourselves to finding the parameters for two the nearest shells. For the data obtained at the Pb absorption edge, we took into account that lead atoms are surrounded by six atoms of two kinds (Se, Te) in the first shell. Each of the Pb–Te and Pb–Se atomic pairs is characterized by its own set of structural parameters (R_j , N_j , σ_j^2). The second shell consists of twelve Pb atoms that were thought to be located at the same distance.¹ In order to decrease the number of the fitting parameters, the relative contributions of the Pb–Te and Pb–Se pairs into the theoretical $\chi(k)$ curves were taken according to the known chemical composition of the samples, and the relative contributions of the first and second shells were taken in accordance with their coordination numbers. The total number of the fitting parameters that describe the local environment of lead was 8.

For the data obtained at the Se absorption edge, we took into account that the first shell of Se always consists of six Pb atoms, while the second shell can contain either Se or Te atoms. It is important to note that the numbers of Se and Te atoms in the second shell may differ from the statistical values because of the manifestation of the short-range order in the solid solution. Thus, we analyzed our data in both approximations, for random and nonrandom distributions of chalcogen atoms in the solid solution.

In the case of a statistical distribution of chalcogen atoms, the problem was limited to finding a set of eight parameters characterizing the local environment of Se atoms in the solid solution.²

In order to take into account a possible nonrandom chalcogen distribution in the second shell, an additional fitting parameter, $N_{\text{Se-Se}}$, was introduced, which is the

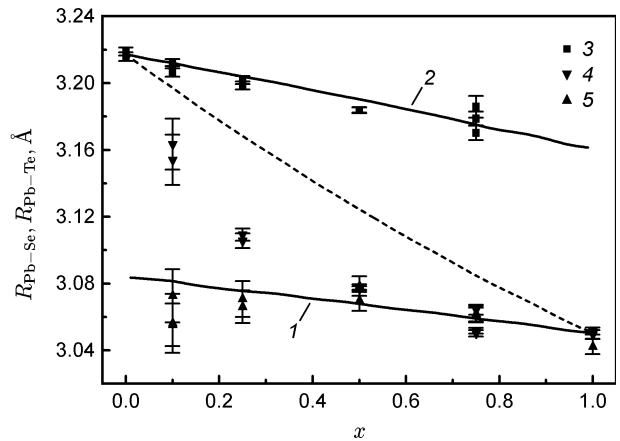


FIG. 3. Pb–Se (1) and Pb–Te (2) bond lengths as a function of composition x of $\text{PbTe}_{1-x}\text{Se}_x$ solid solution. 3, 4, and 5 are the results obtained from the EXAFS data analysis for $R_{\text{Pb-Te}}$, $R_{\text{Pb-Se}}$, and $R_{\text{Se-Pb}}$, respectively. Solid lines and dashed line are mean Pb–Te, Pb–Se distances, and mean interatomic distance (calculated from the lattice parameter) all obtained from the VFF modeling (Sec. 4).

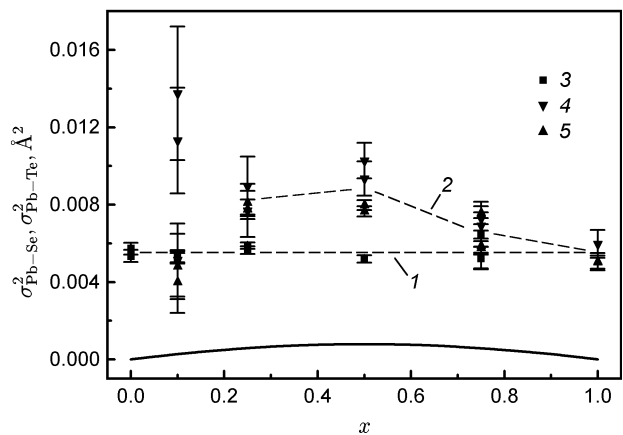


FIG. 4. Debye–Waller factors for Pb–Te (1) and Pb–Se (2) bonds as functions of the composition x of $\text{PbTe}_{1-x}\text{Se}_x$ solid solution. 3, 4, and 5 are the results of the EXAFS data analysis for Pb–Te, Se–Pb, and Pb–Se bonds, respectively. The solid line is the static contribution to the Debye–Waller factor calculated using the VFF method (Sec. 4).

number of Se atoms in the second shell of the central Se atom. We assumed that the total number of atoms in the second shell is always 12.

Taking the possibility of short-range order into account resulted in a considerably better agreement between the experimental and theoretical $k\chi(k)$ curves compared to the model with a random distribution of the chalcogen atoms. The obtained values of $N_{\text{Se-Se}}$ (see Table I) clearly indicate short-range order, namely, the preferential surrounding of Se atoms in the second shell by atoms of the same type. This conclusion is consistent with that of [14], in which the thermodynamic properties of the

¹ Studies of solid solutions with a zinc blende structure [1–3] have shown that the atoms in the second shell can be located at different distances. The justification of the approximation we have made will be given below.

² To determine the parameters more accurately, additional constraints $R_{\text{Se-Te}} = R_{\text{Se-Se}}$ and $\sigma_{\text{Se-Te}}^2 = \sigma_{\text{Se-Se}}^2$ were introduced, and the Te and Se atoms were treated as a single shell. These constraints are justified by earlier studies of solid solutions which revealed a single-mode distribution of bond lengths in the sublattice, in which the isoelectronic substitution takes place [1, 6], and by our VFF modeling of the structure of the $\text{PbTe}_{1-x}\text{Se}_x$ solid solution (see the next section).

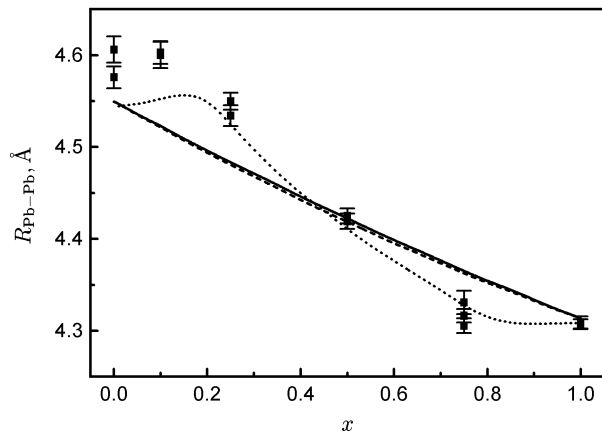


FIG. 5. Pb–Pb interatomic distances as a function of x in the $\text{PbTe}_{1-x}\text{Se}_x$ solid solution. The points are results of the EXAFS data analysis. The solid line is calculated using the VFF method, the dashed line is the mean interatomic distance calculated from the lattice parameter, and the dotted line presents the results of the EXAFS data analysis for simulated $\chi(k)$ curves (equation (4)).

PbTe–PbSe system were studied.

Interatomic distances and Debye–Waller factors for Pb–Te and Pb–Se bonds, derived from analysis of both absorption edges, are plotted as a function of composition x in Figs. 3 and 4.³ Despite the rather large errors in the determination of the Pb–Se distances in samples with low selenium content, the distances obtained at both absorption edges agree well. As follows from Fig. 3, the interatomic bond length distribution in the $\text{PbTe}_{1-x}\text{Se}_x$ solid solution demonstrates a clear bimodal character. The Debye–Waller factor’s dependence on x is different for Pb–Te and Pb–Se bonds (Fig. 4): while $\sigma_{\text{Pb–Te}}^2$ is essentially independent of the composition, $\sigma_{\text{Pb–Se}}^2$ exhibits a maximum near $x = 0.5$. Nevertheless, σ^2 remains below 0.01 \AA^2 for both bond types.

Figs. 5 and 6 show the interatomic distances and Debye–Waller factors as a function of x for second-shell Pb–Pb atom pairs in the $\text{PbTe}_{1-x}\text{Se}_x$ solid solution. Figs. 7 and 8 present the same data for Se–chalcogen atom pairs, taking into account the short-range order. Experimental results indicate a significant deviation from Vegard’s law for the experimental Pb–Pb distance dependence, whereas the Se–chalcogen pairs exhibit a better agreement with Vegard’s law.

The Debye–Waller factors for Pb–Pb and Se–chalcogen atom pairs exhibit similar qualitative trends with respect

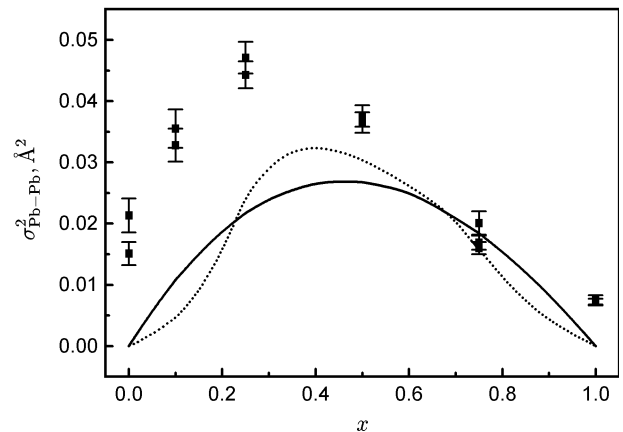


FIG. 6. Debye–Waller factors for Pb–Pb pairs as a function of x in the $\text{PbTe}_{1-x}\text{Se}_x$ solid solution. The points are the results of the EXAFS data analysis. The solid line is the result of the VFF calculations, and the dotted curve presents the results of the EXAFS data analysis for simulated $\chi(k)$ curves (equation (4)).

to x , but their magnitudes differ. The Pb–Pb Debye–Waller factors show a maximum near $x \approx 0.25$ and their values are unexpectedly large (up to 0.05 \AA^2), substantially exceeding those of the Se–chalcogen pairs.

In order to explain the anomalously large Debye–Waller factors for Pb–Pb pairs in $\text{PbTe}_{1-x}\text{Se}_x$, we supposed that the solid solution can transform into a microcoherent state, potentially induced by mechanical treatment during the powder preparation, or the solid solution decomposition due to insufficiently quick cooling of the samples after annealing. To check this supposition, a second set of samples was prepared with the same compositions. Prior to annealing, these samples were ground, and all the annealed powders were quenched from 720°C in cold water. The study of these samples at the Pb L_{III} absorption edge did not reveal any changes in the behavior of the Pb–Pb Debye–Waller factor as a function of x compared to samples of the first series. Moreover, a few samples of the second series were additionally annealed at temperatures from 100 to 400°C to search for changes produced by a possible decomposition. No noticeable changes in the Pb–Pb Debye–Waller factors were found.

To understand the reason for the unusual behavior of the Pb–Pb interatomic distances and Debye–Waller factors (Figs. 5 and 6), we decided to simulate the static distortions in the $\text{PbTe}_{1-x}\text{Se}_x$ solid solution using the valence force field (VFF) method. This method has been used previously [3, 15] to model the structural distortions in semiconductor solid solutions with a zinc blende structure.

³ In the data analysis, we have taken into account systematic errors in the calculations of the theoretical scattering amplitudes and phases by the FEFF software. Distances obtained at the Pb edge were increased by 0.025 \AA [10]. A static correction of 0.5 rad was added to the scattering phase for the Se edge data. These corrections yielded good agreement between EXAFS-derived distances and x-ray data for the reference PbTe and PbSe compounds.

4. VALENCE FORCE FIELD (VFF) MODELING

The static distortions in the $\text{PbTe}_{1-x}\text{Se}_x$ solid solution were modeled within the valence force field (VFF) approximation. For a given random distribution of Se and Te atoms in one of the fcc sublattices, a set of atomic coordinates, $\{\mathbf{r}_i\}$, for which the total strain energy associated with the bond stretching and deviation of the angles between the bonds from 90° ,

$$U = \frac{1}{2} \sum_i \left[\sum_{j=1}^6 A_{s(i,j)} \left(\frac{|\mathbf{r}_i - \mathbf{r}_j| - d_{s(i,j)}}{d_{s(i,j)}} \right)^2 + B \sum_{(j,k)=1}^{12} \left(\frac{(\mathbf{r}_i - \mathbf{r}_j)(\mathbf{r}_i - \mathbf{r}_k)}{|\mathbf{r}_i - \mathbf{r}_j||\mathbf{r}_i - \mathbf{r}_k|} \right)^2 \right], \quad (2)$$

was minimized. In the first term, the sum runs over six nearest neighbors for each lattice site. The indexes $s(i, j) = 1, 2$ denote Pb–Se and Pb–Te pairs with atoms at sites i and j , A_s is the stiffness constant for the corresponding bond, and d_s is its equilibrium length in the binary compound ($d_1 = 3.050$, $d_2 = 3.217$ Å at 80 K). In the second term, the sum runs over all 12 different angles between pairs of bonds for each lattice site. Stiffness constants A_1 and A_2 , associated with the elongation of Pb–Se and Pb–Te bonds, respectively, were derived from published elastic moduli [16] for PbSe and PbTe using the relation $A = (C_{11} + 2C_{12})/4$. The bending stiffness constants were calculated as $B = C_{44}/32$, where C_{44} represents the average shear modulus of PbSe and PbTe.

Simulations were performed on $m \times m \times m$ lattices ($m = 10\text{--}30$) with periodic boundary conditions, employing several realizations of random Se and Te distributions within the chalcogen sublattice. Starting with ideal fcc lattice atomic positions, each atom was displaced in a direction that minimized the strain energy, while maintaining fixed positions of all other atoms. The step size for a single displacement was adaptively reduced from 0.01 to 0.0002 Å. After about 1000 steps per atom, the strain energy U converged, and the resulting atomic configuration was considered as the equilibrium one. Distribution functions for all atomic pairs in the first and second shells were then calculated from the obtained coordinate sets. As the periodic boundary conditions required the lattice parameter to be fixed, the calculations were done for a set of lattice parameters. Its value corresponding to the minimum U was subsequently adopted as the lattice parameter.

Numerical simulations performed on lattices of different size showed that the excess energy due to the finite-size effects scales approximately as m^{-3} and that for $m > 16$, these effects can be neglected.

The calculated mean Pb–Se and Pb–Te bond lengths and their dispersions (static Debye–Waller factors) are represented by solid lines in Figs. 3 and 4. As can be expected, a clear bimodal distribution is observed for the

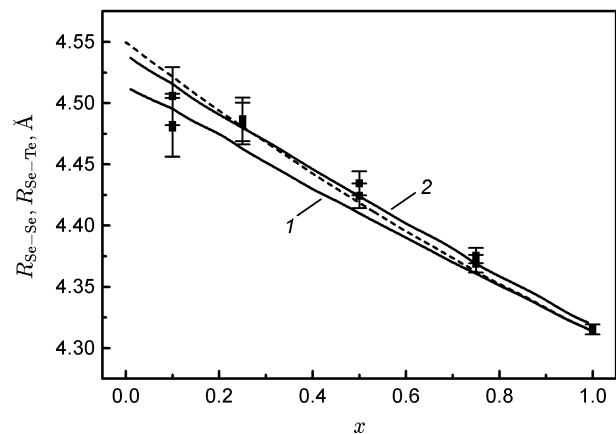


FIG. 7. Se–Se (1) and Se–Te (2) interatomic distances as functions of x in the $\text{PbTe}_{1-x}\text{Se}_x$ solid solution. The points are the results of the EXAFS data analysis. The solid lines are the results of the VFF calculations, and the dashed line is the mean interatomic distance calculated from the lattice parameter.

distances in the first shell. Let us define the relaxation parameter ϵ' for the A – C bond as the variation in its length in two limiting compositions of the $AB_{1-x}C_x$ solid solution, normalized by the total change in the mean interatomic distance,

$$\epsilon' = \frac{R_{AC}^0 - R_{AC}[AB]}{R_{AB}^0 - R_{AC}^0}, \quad (3)$$

where R_{AB}^0 and R_{AC}^0 are the bond lengths in binary AB and AC compounds, and $R_{AC}[AB]$ is the A – C bond length for the impurity C in the AB compound at infinite dilution. For the Pb–Te and Pb–Se bonds, the corresponding values are 0.35 and 0.21, respectively. The difference between the two values of ϵ' is due to an appreciable difference in the bond-stretching constants A_1 and A_2 (about 1.5 times). The value of ϵ' calculated for the Pb–Te bond agrees well with the experimental data ($\epsilon' \approx 0.36$). The comparison for the Pb–Se bond is complicated by larger experimental errors. It is noteworthy that the calculated dependence of the mean interatomic distance on x (dashed line in Fig. 3) displays a noticeable negative bowing compared to Vegard's law (by about 0.009 Å).

Mean interatomic distances and their dispersions calculated for Pb–Pb, Se–Se, and Se–Te pairs in the second shell are presented in Figs. 5 to 8. Very large static Debye–Waller factors in the second shell compared to those in the first shell suggest that the lattice adapts to the existence of different bond lengths by local rotations. The results of VFF simulations for the Se–chalcogen pairs agree well with experimental data, whereas the agreement for the Pb–Pb pairs is not good. The reasons for this disagreement will be discussed in detail in the next section.

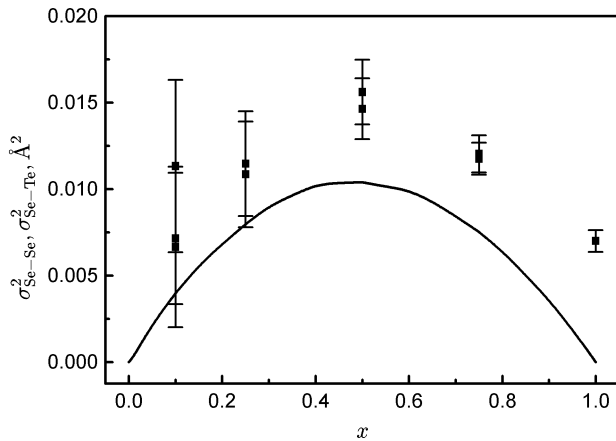


FIG. 8. Debye–Waller factors for Se–Se and Se–Te pairs as functions of x in the $\text{PbTe}_{1-x}\text{Se}_x$ solid solution. The points are the results of the EXAFS data analysis. The solid line is calculated using the VFF method.

Our calculations show that the mean Se–Se distance in the solid solution is only 0.01–0.02 Å shorter than the Se–Te distance (see Fig. 7), and their Debye–Waller factors are nearly equal ($\sigma_{\text{Se–Se}}^2 \approx \sigma_{\text{Se–Te}}^2$). This justifies treating the chalcogen atoms as a unified single shell in our data analysis at the Se edge.

In summary, valence force field modeling of distortions in the $\text{PbTe}_{1-x}\text{Se}_x$ solid solution has predicted inevitably strong static distortions of Pb–Pb distances and demonstrated a qualitative agreement between the calculations and experiment for the first shell and for the Se–chalcogen pairs in the second shell. However, the modeling has not provided an explanation for the discrepancy between the experimentally determined Pb–Pb distances and calculated data, potentially due to the inadequacy of the single-mode approximation for Pb–Pb distances used in the data analysis.

5. DISCUSSION

We start our discussion with a question: Is a single-mode approximation sufficient to describe interatomic distances in the second Pb–Pb shell of the $\text{PbTe}_{1-x}\text{Se}_x$ solid solution?

It has been proposed [1, 17] that the number of modes in the distribution of the A – A distances in an $AB_{1-x}C_x$ solid solution is determined by the number of different ways that link two A atoms, i.e. the distribution should be bimodal for lattices with a zinc blende structure and trimodal for NaCl structure.

That is why we initiated our data analysis by seeking parameters that approximate the distribution function as a sum of a few Gaussians. Unfortunately, a large Debye–Waller factor and a limited k range of EXAFS oscillations did not enable us to determine the param-

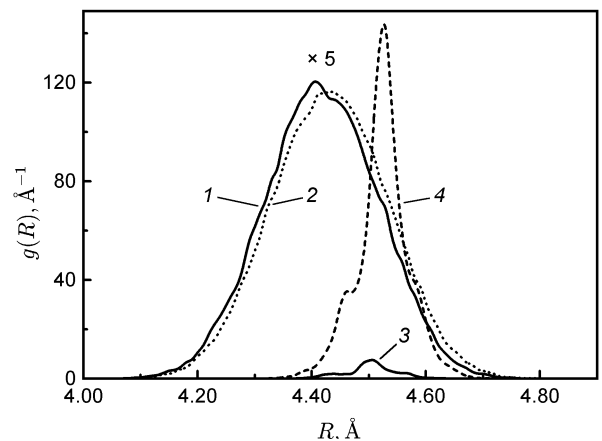


FIG. 9. Se–Se (1, 3) and Se–Te (2, 4) pair distribution functions calculated using the VFF method for the $\text{PbTe}_{1-x}\text{Se}_x$ solid solution with $x = 0.5$ (1, 2) and $x = 0.05$ (3, 4).

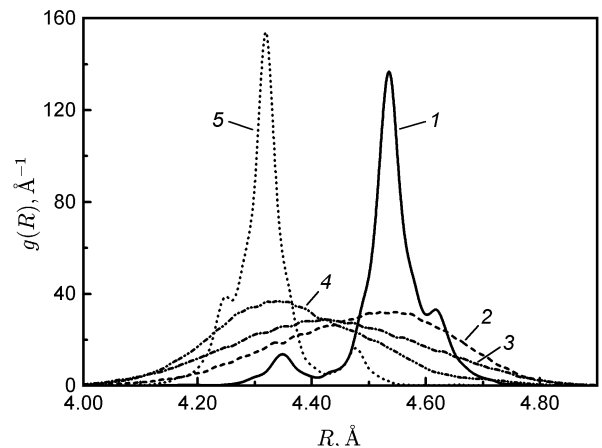


FIG. 10. Pb–Pb pair distribution functions calculated using the VFF method for $\text{PbTe}_{1-x}\text{Se}_x$ solid solution with x : 1 — 0.05, 2 — 0.25, 3 — 0.5, 4 — 0.75, 5 — 0.95.

eters for a trimodal approximation (the solution was not stable). For the bimodal approximation, we succeeded in getting reasonable parameters for compositions close to binary compounds; for the sample with $x = 0.5$, the distance to one of the components became unphysically large (~ 4.7 Å). Since neither the trimodal approximation nor the bimodal one could be used, for all the samples we had to analyze our data using the single-mode approximation.

Let us consider the distribution functions $g(R)$ for Se–Se, Se–Te, and Pb–Pb pairs, calculated using the VFF method (Figs. 9 and 10). It is seen that for $x \approx 0$ and $x \approx 1$, the distribution functions display a fine structure, which is smeared out as $x \rightarrow 0.5$. However, the distribution functions for Se–chalcogen and Pb–Pb pairs are very different. For the Se environment, the mean Se–Se and Se–Te interatomic distances are close, and the distance between the corresponding components in the fine

structure (Fig. 9) is small, typically about the amplitude of thermal vibrations at 80 K. These results confirm the common pattern [1, 6] that the distribution function for a pair of atoms that substitute each other in the solid solution $AB_{1-x}C_x$ can be treated as single-mode.

As follows from Fig. 10, the distribution function for the A - A pair in our solid solution with an NaCl structure cannot be described by the trimodal approximation. Nevertheless, sometimes the fine structure components can be divided tentatively into two groups whose centers of gravity differ significantly. Therefore, it appears that when the smearing is not too large, it is possible to approximate the distribution function by a sum of two Gaussians.

In order to check whether the Pb-Pb distribution functions obtained from the VFF calculations are consistent with the experimental data, we calculated $\chi(k)$ curves using formula

$$\chi(k) = \frac{S_0^2}{k} f(k) \int \frac{g(R)}{R^2} \exp\left(-\frac{2R}{\lambda(k)}\right) \times \sin[2kR + \psi(k)] dR. \quad (4)$$

Then, the calculated curves were analyzed in a way similar to that used for the experimental $\chi(k)$ curves (one distance for the Pb-Pb pair). The interatomic distances and static Debye-Waller factors obtained in this way are plotted with dotted lines in Figs. 5 and 6. It is seen that the obtained data are in good agreement with the experimental data, i.e., the distribution functions calculated using the VFF method provide a qualitatively accurate description of the real structure of the solid solution.

Our results, therefore, show that in the $\text{PbTe}_{1-x}\text{Se}_x$ solid solution, the distortions in the second shell of chalcogen sublattice (where substitution occurs) can be described with sufficient accuracy using a single-mode approximation, whereas for the Pb sublattice (not subject to substitution), it is difficult to find a good working approximation, and the best solution is to use distribution functions calculated using the VFF method.

The experimentally measured Debye-Waller factors are known to consist of static and dynamic terms that correspond to static distortions of the structure and thermal lattice vibrations, respectively. The VFF calculations give only the static part of the Debye-Waller factor. Thus, the difference between the experimental and calculated Debye-Waller factors can be attributed to thermal vibrations. For the first shell (Fig. 4), the dynamic contribution to the Debye-Waller factor is an order of magnitude greater than the static contribution, even at 80 K. The difference in the factors for Pb-Te and Pb-Se bonds is probably related to the appreciable difference in masses of Te and Se atoms. A more detailed analysis of these data is difficult because of the bimodal character of the phonon spectrum of $\text{PbTe}_{1-x}\text{Se}_x$ solid solution [18]. The contribution of thermal vibrations to the Debye-Waller

factor for Se-chalcogen pairs (Fig. 8) in the second shell is a little bit higher than for the first shell (atomic motion in the second shell is less correlated), and within the accuracy of the experiment, it does not depend on x . However, as follows from Fig. 6, for Pb-Pb pairs the dynamic contribution depends on x ; the maximum amplitude of thermal vibrations occurs at $x \approx 0.25$. This result qualitatively agrees with the data of our paper [11], where it was shown that the structure of the $\text{PbTe}_{1-x}\text{Se}_x$ solid solution becomes very “soft” at $x \approx 0.25$, enabling us to observe the onset of the phase transition when a part of Pb atoms are substituted by tin.

We now consider the relaxation of bonds in the solid solution. As shown above, the parameter ϵ' for the $\text{PbTe}_{1-x}\text{Se}_x$ solid solution was ≈ 0.36 , i.e., intermediate between the values observed previously in III-V and II-VI semiconductors with a zinc blende structure (0.05–0.24 [5]) and those in alkali halide crystals with an NaCl structure (≈ 0.5 [17]).

It is obvious that one of the main factors resulting in changes in the bond lengths is the appearance of elastic strain caused by the difference in size of the substituted B and C atoms. As follows from simple considerations [19], the ϵ' value is determined by the crystal structure (mutual position of the atoms in the lattice), so that only the data for the same structures can be compared. Neglecting the bond bending and atomic displacements in the second and more distant shells, the authors of [19] obtained the value of $\epsilon' = 0.25$ for a zinc blende structure and $\epsilon' = 0.5$ for an NaCl structure, assuming equal stiffness for A - B and A - C bonds. More realistic VFF calculations performed in this work, which took the influence of all the factors listed above into account, yielded $\epsilon' = 0.35$ and 0.21 for the two bonds in the $\text{PbTe}_{1-x}\text{Se}_x$ solid solution with an NaCl structure, which is in fair agreement with experiment.

However, the strain contribution alone appears not to be sufficient to explain all the experimental data. Our attempt to calculate ϵ' using the VFF method for the alkali halide $\text{RbBr}_{1-x}\text{I}_x$ and $\text{K}_{1-x}\text{Rb}_x\text{Br}$ crystals with an NaCl structure studied in [17] yielded ϵ' values close to those obtained for $\text{PbTe}_{1-x}\text{Se}_x$, but differing substantially from experiment. A large difference between the experimental values of ϵ' for III-V and II-VI semiconductors with a zinc blende structure and those predicted by the strain model has also been noticed in [5]. In our opinion, these discrepancies are associated with another group of factors which can influence the local structure, namely, the so-called chemical factors, which take into account the individual properties of interacting atoms (their valence, electronegativity), and type of chemical bonding.

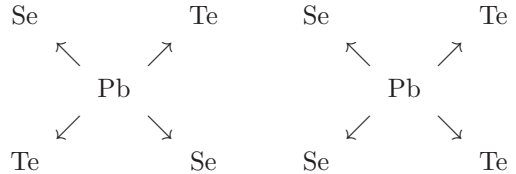
These factors are also manifested in thermodynamic properties; it is known that the enthalpy of mixing of a solid solution, ΔH_m , consists of two components, the strain energy and chemical contribution. The strain en-

ergy U calculated using the VFF method is actually the strain contribution to ΔH_m . In III-V and II-VI semiconductors with a zinc blende structure, the strain energy agrees well with the experimental mixing enthalpy [20]. Unfortunately, the available published data on the enthalpy of mixing of the $\text{PbTe}_{1-x}\text{Se}_x$ solid solution ($\Delta H_m \leq 0.2$ kcal/mole at $x = 0.5$) are not very accurate. Although ΔH_m is positive, thus indicating a tendency to decomposition of the solid solution, the difference between the calculated strain contribution to ΔH_m ($U = 0.38$ kcal/mole) and the measured ΔH_m value may be due to the presence of chemical factors.

Individual members of this group of factors may either increase or decrease the ϵ' values (the chemical bond length). We suppose that in the solid solution under study, the effect of different factors are compensated, and the agreement between the calculated and experimental ϵ' remains good.

From the local concentration of Se-Se pairs (short-range order) obtained in our experiment, the contribution of chemical factors into the mixing enthalpy can be estimated. We define the freezing temperature T_f as a temperature at which the interchange of the two nearest atoms takes one second (it corresponds to the diffusion coefficient of $D = 2 \times 10^{-15}$ cm²/s). According to the published data on the temperature dependence of the diffusion coefficient [21], the estimated value of T_f is 540 K. Using the approximation of pairwise atomic interaction, we calculated the difference between the energy of Se-Te pair and the average energy of Se-Se and Se-Te pairs. This value appeared to be $\Delta E \approx 0.5$ kcal/mole (0.02 eV) for the sample with $x = 0.5$. This value is actually an estimate of the *chemical contribution* into the mixing enthalpy: the atoms in the second shell do not interact elastically, and so there is no elastic contribution to this value. The comparison of the ΔE and U values shows that the chemical and elastic contributions into the mixing enthalpy in the $\text{PbTe}_{1-x}\text{Se}_x$ solid solution have the same order of magnitude.

However, the use of a pairwise atomic interaction approximation is not fully correct, since the atoms in the second shell do not interact directly (either chemically or elastically). So, the appearance of the short-range order is apparently due to some more complex interactions involving three or more atoms. In our experiments, the largest deviations from the random distribution of chalcogen atoms were observed at low Se concentrations and was manifested as the increased number of Se-Pb-Se configurations with Pb-Se bonds oriented at 90°. This suggests that there is an appreciable difference in the energies of configurations in which the like atoms belong to the same or to different p orbitals. These configurations can be schematically shown in the following way:



It cannot be excluded that the cause of such a behavior is associated with unsaturated character of chemical bonds in IV-VI semiconductors.

In conclusion, the use of the VFF method to calculate the bond lengths and pair correlation functions for the first and second shells enables us to describe qualitatively the distortions of the structure in the $\text{PbTe}_{1-x}\text{Se}_x$ solid solution. However, this model does not predict the scatter in the experimental ϵ' values, for which the model predicts close values of this parameter, as well as the appearance of the short-range order. This evidences that along with elastic interactions, the influence of chemical factors should be taken into account to describe the properties of solid solutions.

This work was partially supported by the Russian Foundation for Basic Research (Grant No. 95-02-04644).

-
- [1] J. C. Mikkelsen, Jr. and J. B. Boyce, Extended x-ray-absorption fine-structure study of $\text{Ga}_{1-x}\text{In}_x\text{As}$ random solid solution, *Phys. Rev. B* **28**, 7130 (1983).
 - [2] A. Balzarotti, N. Motta, A. Kisiel, M. Zinnal-Starnawska, M. T. Szyzyk, and M. Podgórnny, Model of the local structure of random ternary alloys: Experiment versus theory, *Phys. Rev. B* **31**, 7526 (1985).
 - [3] N. Motta, A. Balzarotti, P. Letardi, A. Kisiel, M. T. Szyzyk, M. Zinnal-Starnawska, and M. Podgórnny, EXAFS of $\text{Cd}_{1-x}\text{Zn}_x\text{Te}$: A test of the random distribution in zincblende ternary alloys, *Solid State Commun.* **53**, 509 (1985).
 - [4] W.-F. Pong, R. A. Mayanovic, B. A. Bunker, J. K. Furdyna, and U. Debska, Extended x-ray-absorption fine-structure studies of $\text{Zn}_{1-x}\text{Mn}_x\text{Se}$ alloy structure, *Phys. Rev. B* **41**, 8440 (1990).
 - [5] R. A. Mayanovic, W.-F. Pong, and B. A. Bunker, X-ray-absorption fine-structure studies of $\text{Hg}_{1-x}\text{Cd}_x\text{Te}$ and $\text{Hg}_{1-x}\text{Mn}_x\text{Te}$ bond lengths: Bond relaxation and structural stability of ternary alloys, *Phys. Rev. B* **42**, 11174 (1990).
 - [6] Z. Wu, K. Lu, Y. Wang, J. Dong, H. Li, C. Li, and Z. Fang, Extended x-ray-absorption fine-structure study of $\text{GaAs}_x\text{P}_{1-x}$ semiconducting random solid solutions, *Phys. Rev. B* **48**, 8694 (1993).
 - [7] Q. Islam and B. A. Bunker, Ferroelectric transition in $\text{Pb}_{1-x}\text{Ge}_x\text{Te}$: Extended x-ray-absorption fine-structure investigation of the Ge and Pb sites, *Phys. Rev. Lett* **59**, 2701 (1987).
 - [8] B. A. Bunker, Q. Islam, and W.-F. Pong, The ferroelectric transition in IV-VI semiconductor alloys, *Physica B* **158**, 578 (1989).

- [9] Z. Wang and B. A. Bunker, X-ray-absorption fine-structure studies of $\text{PbS}_x\text{Te}_{1-x}$ alloys: Ferroelectric phase transitions induced by off-center ions, *Phys. Rev. B* **46**, 11277 (1992).
- [10] A. I. Lebedev, I. A. Sluchinskaya, V. N. Demin, and I. H. Munro, Off-centering of Pb and Sn impurities in GeTe, *Phys. Rev. B* **55**, 14770 (1997).
- [11] A. I. Lebedev and I. A. Sluchinskaya, Structural disorder and phase transition in $\text{Pb}_{1-x}\text{Sn}_x\text{Te}_{1-y}\text{Se}_y$, *Fiz. Tverd. Tela* **32**, 1780 (1990).
- [12] P. A. Lee, P. H. Citrin, P. Eisenberger, and B. M. Kincaid, Extended x-ray absorption fine structure—its strengths and limitations as a structural tool, *Rev. Mod. Phys.* **53**, 769 (1981).
- [13] J. Mustre de Leon, J. J. Rehr, S. I. Zabinsky, and R. C. Albers, *Ab initio* curved-wave x-ray-absorption fine structure, *Phys. Rev. B* **44**, 4146 (1991).
- [14] Shamsuddin and S. Misra, On the thermodynamic properties of PbTe–PbSe system, *Z. Metallkd.* **70**, 541 (1979).
- [15] M. Podgórný, M. T. Szyzyk, A. Balzarotti, P. Letardi, N. Motta, A. Kisiel, and M. Zimnal-Starnawska, Crystallographic structure of ternary semiconducting alloys, *Solid State Commun.* **55**, 413 (1985).
- [16] O. Madelung, M. Schulz, and H. Weiss, eds., *Landolt-Börnstein. Numerical data and functional relationships in science and technology. New Series. Group III.*, Vol. 17f (Springer-Verlag, 1983).
- [17] J. B. Boyce and J. C. Mikkelsen, Jr., Local structure of ionic solid solutions: Extended x-ray-absorption fine-structure study, *Phys. Rev. B* **31**, 6903 (1985).
- [18] H. Finkenrath, G. Franz, and N. Uhle, Reststrahlen spectra of $\text{PbSe}_{1-x}\text{Te}_x$, *Phys. Status Solidi (B)* **95**, 179 (1979).
- [19] C. K. Shih, W. E. Spicer, W. A. Harrison, and A. Sher, Bond-length relaxation in pseudobinary alloys, *Phys. Rev. B* **31**, 1139 (1985).
- [20] Z. Wu and K. Lu, Local structures in zinblend-type random solid solutions, *J. Phys. Condens. Matter* **6**, 4437 (1994).
- [21] M. Schulz and H. Weiss, eds., *Landolt-Börnstein. Numerical data and functional relationships in science and technology. New Series. Group III.*, Vol. 17d (Springer-Verlag, 1984).